Catalysis Today 345 (2020) 227–236

Contents lists available at ScienceDirect

Catalysis Today

journal homepage: www.elsevier.com/locate/cattod

Highly active hybrid mesoporous silica-supported base organocatalysts for C—C bond formation

A. Erigoni, M.C. Hernández-Soto, F. Rey, C. Segarra*, U. Díaz*

Instituto de Tecnología Química, Universitat Politècnica de València-Consejo Superior de Investigaciones Científicas, Avenida de los Naranjos s/n, E-46022, Valencia, Spain

ARTICLE INFO

Keywords:
Organic-inorganic hybrid catalysts
Base sites
Mesoporous and microporous materials
C—C bond forming reactions

ABSTRACT

New base hybrid catalysts, based on silyl-derivatives of molecules carrying amino, diamino, pyrrolidine, pyrazolium and imidazolium functionalities have been successfully achieved through post synthetic grafting onto M41S-type support. Different characterization techniques were implemented to study the characteristics of the materials, such as elemental analysis, solid state MAS NMR and FTIR spectroscopies, X-ray diffraction (XRD), thermogravimetric and differential thermal analyses (TGA-DTA) and textural properties through N_2 physisorption analysis. The catalytic activity and recyclability of these compounds as base catalysts was demonstrated for C—C bond forming reactions such as Knoevenagel condensations and Michael additions rationalizing the differences observed as function of the reaction mechanisms. An enamine mechanism was proposed for Knoevenagel condensations and an enolate mechanism for Michael additions.

1. Introduction

In the last years, the design of new hybrid organic-inorganic catalysts based on organocatalysts incorporated into the framework of conventional inorganic supports is becoming an area of growing interest due to their specific physical and chemical properties. The use of these hybrid catalysts allows combining increased flexibility, functionality and efficiency of soluble organic homogeneous catalysts, with the thermal and mechanic stability of inorganic solids, leading to 'green catalytic processes', with higher selectivity and conversion and easy catalyst recovery [1–3].

Different routes can be followed to synthesise organic–inorganic hybrid catalysts that include: adsorption of the organic species inside the pores of the inorganic host, inclusion of the organic moieties within the pores of the support by a "ship in a bottle" type procedure, one-pot synthesis of a composite material with the organic fragments located into the walls of the pores by hydrolysis and condensation routes, and post-synthetic grafting of the organic moieties onto the surface of the inorganic support [4–6].

Post-grafting of silica surfaces using functionalized organosilanes is one of the most extensively used methods, primarily due to its versatility and to the avoidance of the synthetic step related to the extraction of the surfactant from the pore channels, typical of most synthesis carried out following one-pot approaches [7,8]. Nevertheless, an optimal grafting procedure must keep into account the possibility of partial pores blockage and the undesired oligomerization of the silylated organic precursors [9–11]. In the design of hybrid organic-inorganic catalysts, silica-based materials are the most implemented supports, due to their highly reactive surface, tunable pore size and relatively high thermal and mechanic stability [12]. Moreover, weakly acidic silanols present of the surface of the support have been shown to play an important role in both enhancing or inhibiting the catalytic activity of the pending active sites, depending on the specific reaction [13–16]. Additionally, the range of alkoxysilanes that can be grafted to the surface silanols allows for a highly tunable series of organic moieties that can be tethered to the surface to catalyze the desired reaction [17–19].

Specifically, the synergistic effect of base active sites and acidic surface silanol groups in promoting aldol condensation reactions have been thoroughly studied [20–22]. Several authors reported that capping the silanols with methyl groups greatly affected the activity of the hybrid catalysts [23,24]. On the other hand, the presence of more strongly acidic active sites (i.e. carboxylic acids), together with the amine, was shown to provide lower catalytic activity, probably due to the fact that stronger acidity would make the proton transfer to the amine more likely to occur, ultimately causing the deactivation of the base catalytic sites [25]. The influence of the length of the linker is also a key factor in designing a such silica-supported base catalysts: flexible linkers (C3 or longer) allows for the amine to get into close proximity of the silanols, enabling their cooperation in catalysing the reaction [26].

* Corresponding authors.
E-mail addresses: canseal@itq.upv.es (C. Segarra), udiaz@itq.upv.es (U. Díaz).

https://doi.org/10.1016/j.cattod.2019.09.041
Received 1 July 2019; Received in revised form 3 September 2019; Accepted 25 September 2019
Available online 08 October 2019

Nevertheless, for mesoporous hybrids with a pore diameter of about 2 nm, linkers that are longer than C3 were reported to be detrimental for the catalytic activity [27]. Additionally, for the aldol condensation, different researches postulated sequential activation of the ketone (electrophile) to form the reactive enamine intermediate using a single silanol, which then attacks the aldehyde [28–30].

In this work, organic–inorganic hybrid materials based on silyl-derivatives with base functionalities as amino, diamino and pyrrolidine molecules, pyrazolium and imidazolium hydroxides have been successfully achieved through post synthetic grafting on the surface of pure silica M41S-type support. Based on the consideration mentioned above, a propyl chain was chosen as linker (both when using commercial and non-commercial silyl-derivatives) as it was shown to be the optimal length for amines grafted within pore channels with a diameter of about 2 nm. The synthesized hybrids materials were extensively characterized and tested as base catalysts for the Knoevenagel condensation of benzaldehyde with compounds containing activated methylenic groups. From the catalytic results an imine/enamine mechanism was proposed to follow the reaction and several catalyst recycles were performed to evaluate catalyst deactivation and reusability. These catalysts were studied also in the Michael addition of ethyl 2-oxocyclopentane 2-carboxylate and methyl vinyl ketone and an enolate mechanism is proposed from the data in catalysis,

2. Experimental section

2.1. Catalysts preparation

2.1.1. Synthesis of MCM-41

MCM-41 was synthesized according to a previous report [31]. Cetyltrimethylammonium bromide (13.66 g, 7.6 mmol) was dissolved in distilled water (91 mL) with an aqueous tetramethylammonium hydroxide solution (25 wt %, 23.66 g) in a 250 ml flask at 40 °C. The mixture was stirred vigorously. Aerosil 200 (15 g) was added and the mixture was stirred for 1 h. The gel is then transferred into a stainless steel autoclave and reacted under static condition at 135 °C for 24 h. The resulting solid was filtered and washed several times with distilled water, and the powder was dried at 100 °C in an oven overnight. The powder was calcined under a flow of N_2, ramped from room temperature to 540 °C at 3 °C/min and held at 540 °C for 1 h. Subsequently, the powder was held at the same temperature under a flow of air for 6 h and finally the sample was cooled to room temperature for 2 more extra hours (10 °C/min).

2.1.2. Synthesis of the silylated base precursors III, IV, V and VI

III. 2-aminopyrrolidine (2.32 mmol, 200 mg) and 3-isocyanatopropyltriethoxysilane (2.32 mmol, 564 mg) were placed in a Schlenck under N_2 containing dry CH_3CN and the solution was stirred at -57 °C for 6 h. After this time, the solvent was removed under reduced pressure and the resulting gel was washed with ether (Scheme 1a).

IV-VI. The corresponding amount of the azol compound (1.3 mmol, 110 mg for 1-methylpyrazole and 1-methylimidazol and 128 mg for 1,2-dimethylimidazol) and 3-iodopropyltrimethoxysilane (1.3 mmol, 387 mg) were placed in a round bottomed flask under N_2 containing dry CH_3CN and the solution was refluxed overnight. After this time, the solvent was removed under reduced pressure and the resulting gel was washed with ether (Scheme 1a).

2.1.3. Grafting of the silyl-derivatives on MCM-41

1-3 (4 mol %): MCM-41 (2 g) was placed in a Schlenck under vacuum at 150 °C for 2 h. Dry toluene was added into the Schlenck and the mixture was stirred at RT for 1 h. After that, the corresponding amount of silyl base precursor (1.3 mmol, 295 mg for APTES **I**, 297 mg for N-(2-Aminoethyl)-3-(trimethoxysilyl)propylamine **II** and 445 mg for **III**) was added and the resulting mixture was refluxed for 24 h. After this time, the mixture was filtrated and washed with toluene, CH_2Cl_2 and ethanol and the resulting solid was dried overnight at 100 °C (Scheme 1b).

4-6 (4 mol %): MCM-41 (2 g) was placed in a Schlenck under vacuum at 150 °C for 2 h. Dry CH_3CN was added into the Schlenck together with the corresponding amount of the silyl-derivative (1.3 mmol, 496 mg for **IV** and **V** and 515 mg for **VI**), and the mixture was stirred at room temperature for 1 h. After that, trimethylamine (1.3 mmol, 186 μL) was added and the resulting mixture was refluxed for 24 h. Next, the mixture was filtrated and washed with CH_3CN and acetone and the resulting solid was treated three times with a methanol solution of TMAOH (0.2 M) at room temperature for 30 min to exchange the halogen for hydroxide groups. The final solid was washed abundantly with distilled H_2O and acetone and dried overnight at 100 °C (Scheme 1b).

2.1.4. Syntheis of 1-HMDS

1 (0.5 g) was placed in a Schlenck, outgassed at 150 °C for 2 h. Meanwhile, a solution of hexamethyldisilazane (HMDS,1.25 mmol, 202 mg) in DMF (83.3 mmol, 6.1 mL) was prepared under N_2. After the outgassing, **1** was cooled at room temperature and the HMDS solution was added in the Schlenck. The final composition of the mixture was SiO_2 : 0.15 HMDS : 10 DMF. The mixture was stirred at 120 °C for 2 h. The samples was filtered, washed with CH_2Cl_2 and dried overnight at 100 °C.

2.2. Characterization techniques

XRD analysis was carried out with a Philips X'PERT diffractometer equipped with a proportional detector and a secondary graphite monochromator. Data were collected stepwise over the $2^\circ \leq 2\theta \leq 20^\circ$ angular region, with steps of 0.02° 2θ, 20 s/step accumulation time, and Cu Kα (λ = 1.54178 Å) radiation. C, N, S, and H contents were determined with a Carlo Erba 1106 elemental analyzer. Thermogravimetric and differential thermal analyses (TGA-DTA) were conducted in an air stream with a Mettler Toledo TGA/SDTA 851E analyzer. Nitrogen adsorption isotherms were measured at −196 °C with a Micromeritics ASAP 2010 volumetric adsorption analyzer. Before the measurements, the samples were outgassed for 12 h at 100 °C. The BET specific surface area [32] was calculated from the nitrogen adsorption data in the relative pressure range from 0.04 to 0.2. The total pore volume [33] was obtained from the amount of N_2 adsorbed at a relative pressure of about 0.99. External surface area and micropore volume were estimated using the t-plot method in the t range from 3.5 to 5. The pore diameter and the pore size distribution were calculated using the Barret − Joyner − Halenda (BJH) [34] method on the adsorption branch of the nitrogen isotherms. Solid state MAS NMR spectra were recorded at room temperature under magic angle spinning (MAS) in a Bruker AV-400 spectrometer. The single pulse ^{29}Si spectra were acquired at 79.5 MHz with a 7 mm Bruker BL-7 probe, using pulses of 3.5 μs corresponding to a flip angle of 3/4 π radians and a recycle delay of 240 s. The 1H to 13C crosspolarization (CP) spectra were acquired by using a 90° pulse for 1H of 5 μs, a contact time of 5 ms, and a recycle of 3 ms. The ^{13}C spectra were recorded with a 7 mm Bruker BL-7 probe and at a sample spinning rate of 5 kHz. ^{13}C and ^{29}Si were referred to adamantine and tetramethylsilane, respectively. Liquid state ^{13}C NMR spectra were recorded at 75 MHz using a Bruker AMX300 instrument. Chemical shifts are quoted in ppm and are referenced to the appropriate residual solvent peak.

2.3. Catalytic tests

2.3.1. Knoevenagel condensation

The reaction was carried out in high pressure pyrex tubes with constant magnetic stirring. A mixture of benzaldehyde (1.0 mmol, 106 mg) with ethyl cyanoacetate (1.0 mmol, 113 mg) or ethyl acetoacetate (1.0 mmol, 130 mg) or diethyl malonate (1.0 mmol, 160 mg), anisole (as internal standard,1 mmol) and base catalyst (10 mol % or

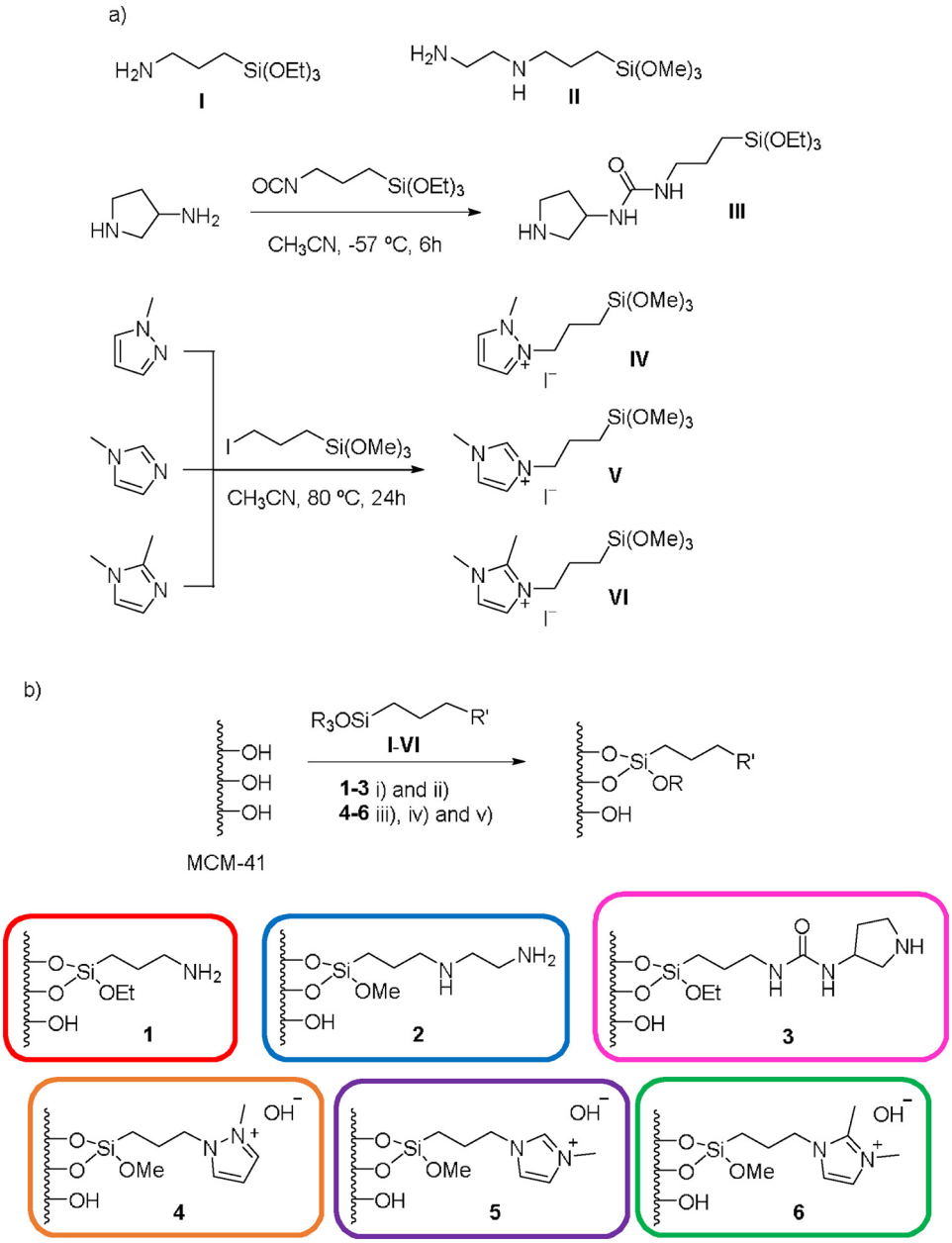

Scheme 1. a) Scheme of 3-triethoxysilylpropylamine (APTES) **I** and N-(2-Aminoethyl)-3-(trimethoxysilyl)propylamine **II** and synthesis of the silylated base precursors **III**, **IV**, **V** and **VI**. **b)** Synthetic steps implemented in the synthesis of the silica-supported base catasyts **1–6.** i) MCM-41, dry Toluene, 1 h, RT; ii) silylated base precursor **I**, **II** or **III**, 24 h, reflux; iii) MCM-41, silylated base precursor **IV**, **V** or **VI**, dry CH_3CN, 1 h, RT, iv) TEA, reflux, 24 h; v) TMAOH, CH_3OH, 30 min.

2 mol % active site), was refluxed at 80 °C in 4 ml of acetonitrile for 24 h. The reaction was monitored by NMR analysis using $CDCl_3$ as deuterated solvent.

2.3.2. Michael addition

In a glass microreactor (2 mL) with a magnetic stir bar, ethyl 2-oxocyclopentane 2-carboxylate (1.0 mmol, 156 mg,), methyl vinyl ketone (1.0 mmol, 70 mg), 4-chlorotoluene (as internal standard, 1 mmol, 126 mg,) and base catalyst (5 mol % active site), was stirred at room temperature in 0.5 ml of CH_3CN for 3 h. The reaction was monitored by NMR analysis using d_3-CD_3CN as deuterated solvent.

3. Results and discussion

3.1. Synthesis of the hybrid mesoporous base catalysts

Firstly, the non-commercial silylated base precursors were synthesized starting from cheap and readily available 1-methylpyrazole, 1-methylimidazol and 1,2-dimethylimidazol through thermally induced condensation with 3-iodopropyltrimethoxysilane giving **IV**, **V** and **VI**, respectively. In the case of **III**, the condensation between 2-aminopyrrolidine and 3-isocyanatopropyltriethoxysilane was carried out at -57 °C in order to inhibit the reaction of the isocyanate with the secondary amine in the **N**-heterocycle. The silylation processes were followed by liquid (^1H, ^{13}C, ^{29}Si) NMR (see Fig. S1 for ^1H NMR spectra, ^{13}C and ^{29}Si NMR spectra are shown in Figs. 2 and 3, respectively). In particular, the ^1H NMR spectra of the silylated base precursors **IV**, **V** and **VI** show the signals assigned to CH groups of the azolium ring at

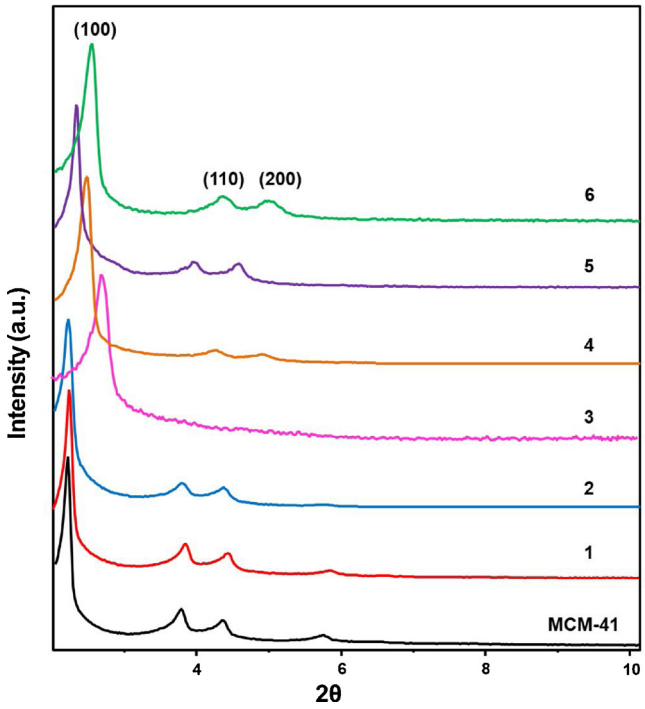

Fig. 1. Powder XRD diffraction patterns of the bare MCM-41 silica and the silica-supported base catalysts **1–6**.

higher chemical shifts compared to those of the corresponding azol rings, due to the un-shielding effect given by the presence of the positive charge. For **III**, the ^{13}C NMR spectrum shows the characteristic signal corresponding to the carbonyl urea group confirming the condensation of the cyano group. The silylated base precursors were then grafted onto MCM-41 support, to give the hybrid base catalysts **1-6** (Scheme 1b).

3.2. Characterization of the hybrid mesoporous base catalysts

The silica-supported base catalysts were characterized by X-ray diffraction (Fig. 1). The diffractograms of all the samples exhibits the (100) reflection peak at low diffraction angles (2θ = 2.3–2.6°) and the (110) and (200) reflections at 2θ = 3.8–4.8°, indicating the preservation of the 2D hexagonal structure of the MCM-41 throughout the grafting procedure and the exchange in basic pH. [35,36] Focusing on the (100) peak, a slight difference in its position can be observed in the samples. This is partly due to the different size of the pending moieties, which affects the mean pore diameter to a different extent and therefore cause a displacement of the peak proportional to the size of the pending moieties. Nevertheless, a full understanding of these features should keep into account the bending of the organic moieties and their interaction with the surface of the support.

The presence of the silylated base precursors in the synthesized hybrid materials was determined by means of elemental analysis. The C, H, N contents and the calculated percentage in weight of the organic moieties present in the silica-supported base materials are summarized in Table 1. The organic content of the hybrid materials increases according to the molecular weight of the silylated base precursor. Thus, the highest organic content corresponds to catalyst **3** (10.4%), where the molecular weight of the organic moiety **III** is 333.5 g/mol. Accordingly, the smallest organic content corresponds to catalyst **1** (4.4%), where the molecular weight of the organic moiety **I** is 221.37 g/mol. Lastly, the organic content for catalyst **4** and **5** is practically the same (8.3 and 8.6, respectively), being the molecular weight of both organic moieties **IV** and **V** is 362.38 g/mol. The amount of N allowed for the determination of the quantity of active sites per gram. Minor differences in the active base sites loading were observed between the six catalysts (Table 1).

Table 1
Organic content in the mesoporous hybrid materials estimated by elemental analysis.

Catalysts	N%	C%	Organic content (EA)%	Active sites (mmol/g)[a]
Cat. 1	1.1	3.3	4.4	0.786
Cat. 2	2.4	5.8	8.2	0.857
Cat. 3	2.5	7.9	10.4	0.595
Cat. 4	1.9	6.3	8.3	0.678
Cat. 5	2.0	6.6	8.6	0.714
Cat. 6	2.0	7.3	9.3	0.714

[a] Active sites = N% / 14 / 100 / n_N. n_N = number of nitrogen atoms present in the sylil-derivative compound.

Thermogravimetric analysis was performed in order to gain insights about the thermal stability of organic units introduced in the hybrid materials. The weight loss (TGA) and its respective derivative curves (DTA) for the silylated base catalysts **1-6** are shown in Fig. S2. In all cases, a first weight loss due to the removal of physisorbed water is observed at around 90–150 °C. The decomposition of the organic moieties occurs in the range between 200–400 °C for all samples. In all the hybrids, a progressive weight loss at temperatures above 500 °C was detected due to dehydroxylation phenomena, i.e. condensation of external silanol groups with the release of water molecules and formation of strained siloxane bridges.

To study the integrity of the organic moieties in the final solid catalysts and specifically the covalent insertion of the silylated base precursor into the structure of the MCM-41 support, solid state MAS NMR spectroscopy was implemented. ^{13}C CP/MAS NMR spectra of all the hybrid base materials were recorded and compared to the spectra recorded on the silyl-derivatives prior grafting (liquid NMR) (Fig. 2a–f). In all cases, the ^{13}C spectra of the hybrids present the typical signals of the silylated-derivatives confirming the integrity of the organic moieties after the synthesis process. Specifically, the ^{13}C peaks due to the propyl chains appear in the range 0–70 ppm for **1-6**, while the peaks corresponding to the rest of the carbon atoms of catalyst **2** and **3** appear in the same range, with the exception of the characteristic C═O signal of catalyst **3** that is visible at 160 ppm. For catalysts **4**, **5** and **6** the signal due to the methyl group NCH_3 appears at a range of 33–36 ppm. The rest of aromatic signals corresponding to the azol rings are visible at the expected range between 107–142 ppm (see the inset in Fig. 2 for the labels of C atoms).

^{29}Si MAS NMR spectra of the hybrids mesoporous base materials **1-6** (Fig. 3a–f) exhibit bands from -50 to -80 ppm assigned to T-type silicon species corresponding to silicon atoms directly bounded to carbon atoms, confirming that the grafting of silylated-derivatives occurs through alkoxy terminal groups of the silylated moieties which react with external silanol groups present onto the inorganic surface support. Comparison of ^{29}Si NMR spectra of the hybrids with the silylated base precursors (see the inset of Fig. 3) confirms also the incorporation of the organic molecules into the framework of non-ordered mesoporous silica. Silylated-derivatives **I**, **II**, **V** and **VI** exhibit a peak centred at around – 43 ppm which, after the grafting, is shifted in the range -50 to -80 ppm, supporting the covalent incorporation of the silylated organic species into the silica framework. Additionally, the presence of the support gives rise to Q-type signals related to bulk and surface silicon atoms. Specifically, three peaks at -92, -100 and -110 ppm are present, due to Q^2 ($Si(OH)_2(OSi)_2$), Q^3 ($Si(OH)(OSi)_3$) and Q^4 ($Si(OSi)_4$) silicon units, respectively. [37] The integration of T and Q peaks in the ^{29}Si BD/MAS NMR spectra was performed to calculate the T/(Q + T) ratio and to evaluate the number of functionalized silicon atoms in the hybrids (Table 2). The Si_{func}/Si_{tot} ratio evidences that the percentage of grafting achieved in this catalysts is the range 1.9–4.7 mol% respect to total silica.

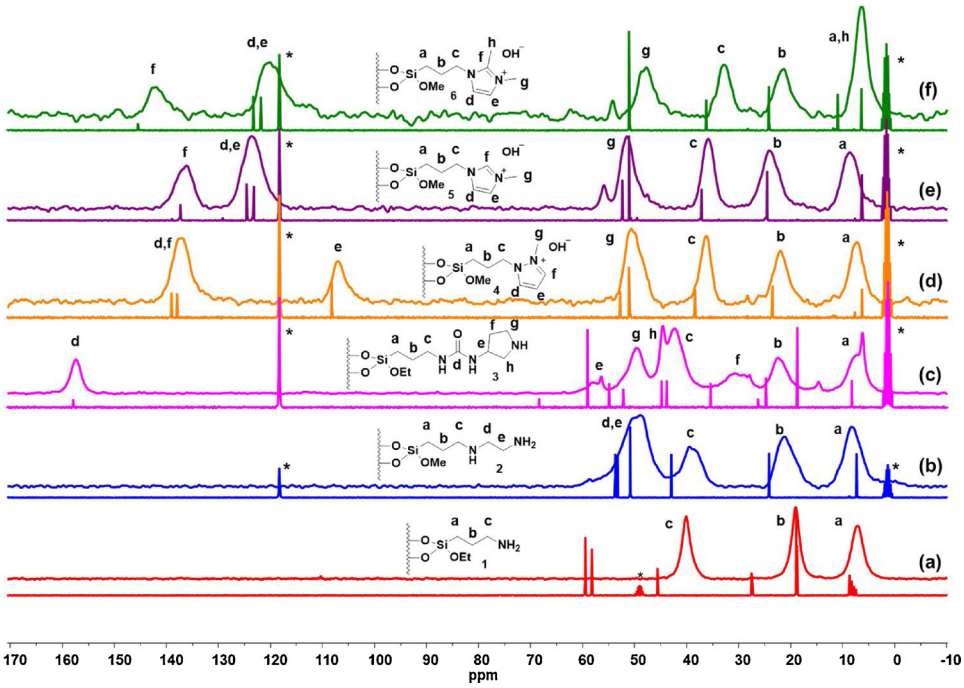

Fig. 2. ^{13}C CP/MAS NMR spectra of the hybrid base catalyst and the silyl-derivatives counterparts: (a) catalyst **1** and silyl-derivative **I**, (b) catalyst **2** and silyl-derivative **II**, (c) catalyst **3** and silyl-derivative **III**, (d) catalyst **4** and silyl-derivative **IV**, (e) catalyst **5** and silyl-derivative **V** and (f) catalyst **6** and silyl-derivative **VI**. *Solvent residual peak.

FTIR spectra were recorded on the base hybrids, after outgassing at 120 °C for 2 h (Fig. 4). Focusing on the high frequency region of the spectra, a signal at 3740 cm^{-1} is observed in all six catalysts and bestowed to the stretching modes of isolated silanols. A broad signal centred between 3700 and 3500 cm^{-1} is ascribed to the stretching modes of hydroxyl groups in interaction with each other through H-bond. Additionally, in the ionic hybrids (spectra 4–6), a component of this composite band stands out at about 3650 cm^{-1} which is bestowed to the stretching modes of the hydroxyl anions present as counter ion. Spectra 1 and 2 show two signals centred at about 3370 and 3310 cm^{-1} related to the asymmetric and symmetric stretching modes of the N—H bond, respectively. In the same region of the spectrum of catalyst 3, a composed signal is observed between 3500 and 3260 cm^{-1}, due to the presence of N—H stretching modes in the urea group (about 3440 cm^{-1}) and in the pyrrolidine ring (asymmetric at 3365 cm^{-1}; symmetric at 3300 cm^{-1}). Spectra of hybrid 4–6 show composite signals between 3200 and 3000 cm^{-1}, bestowed to the alkene C—H stretching modes, in the azo-cycles. In the region comprised between 3000-2840 cm^{-1}, signals related to the alkane C—H stretching modes are observed in all six spectra. [38]

Due to the similar chemical structure, the low frequency region of the spectra recorded on catalyst 1 and 2 show resembling features: a peak centered at 1590 cm^{-1} due to the primary amine N—H bending modes is observed in both spectra; moreover, a week signals at 1460 cm^{-1} is seen and ascribed to the scissor vibration modes of the CH_2 groups present in the propyl chain. In the spectrum of catalyst 3, two intense and partially overlapped bands are visible at 1635 and 1605 cm^{-1}. The first one is bestowed to the stretching modes of the carbonyl C—O bonds in the urea group (Amide I band), whereas the second one is related to the amide II band, i.e. a motion combining N—H bending and C—N stretching of the amide group. Additionally, a band at 1535 cm^{-1} is observed and tentatively ascribed to the N—H bending modes in the pyrrolidine ring. In the region between 1490 and 1370 cm^{-1} signals related to R-C—H bending modes of species (where R is either a nitrogen or a carbon atom) are observed. Due to the lack of spectroscopic data reported in the literature and to the complex nature of the pyrazolium ion, no specific assignation of the signal present in the low frequency region of spectrum 4 was possible. [38]

The low frequency region of the spectra recorded on the imidazolium-derivative catalysts (5 and 6) show similar spectroscopic features. Firstly, a signal related to a motion combining C4–C5 and C—N stretching is present at 1570 cm^{-1} (spectrum 5) and 1585 cm^{-1} (spectrum 6); Moreover, a signal centred at about 1480 cm^{-1} is bestowed to the CH_3(N1) scissoring modes. The spectrum of hybrid 6 also show a typical band related to the N_1-C_2-N_3 stretching + CH_3(C2) rocking modes centred at about 1535 cm^{-1} [39].

3.3. Textural properties

The textural properties of the hybrid materials **1–6** studied by means of N_2 physisorption analysis at 77 K are reported in Table 3 and compared to a pure MCM-41. In all cases, the isotherms show a type IV behavior, with a hysteresis loop, typical of mesoporous materials (Fig. 5). The N_2 uptake is consistent with MCM-41-type materials. In particular, all the hybrids mesoporous catalysts show an isotherm with the inflexion point between p/p_0 0.2–0.3 while the inflexion point of the silica is observed at higher p/p_0 value, meaning that the pore diameter is slightly larger than for the hybrids materials. By analysing the isotherms by the Brunauer-Emmett-Teller (BET) method, specific surface areas (SSA) in the range between 844–1159 m^2/g were observed. The pore volume of the hybrids and of the purely inorganic support were calculated by means of the Barrett-Joyner-Halenda (BJH) method (Table 3). Upon grafting, the BJH pore volume drops from 0.8 to 0.4-0.5 cm^3/g, due to the presence of the pending organic moieties, which partially block the free porous volume.

3.4. Catalytic activity

as base catalysts, hybrids **1-6** were tested in the condensation of carbonyl compounds with active methylenic substrates, in reactions such as Knoevenagel condensation and Michael addition. These reactions are a key tool in organic synthesis for C—C bond formation and for the synthesis of substituted alkene products which are of great interest to produce important intermediates and final products for perfumes, pharmaceutical, dyes and polymers, [40–44] due to their properties as enzyme inhibitors, antitumor, anti-inflammatory, and antibacterial agents [45–48].

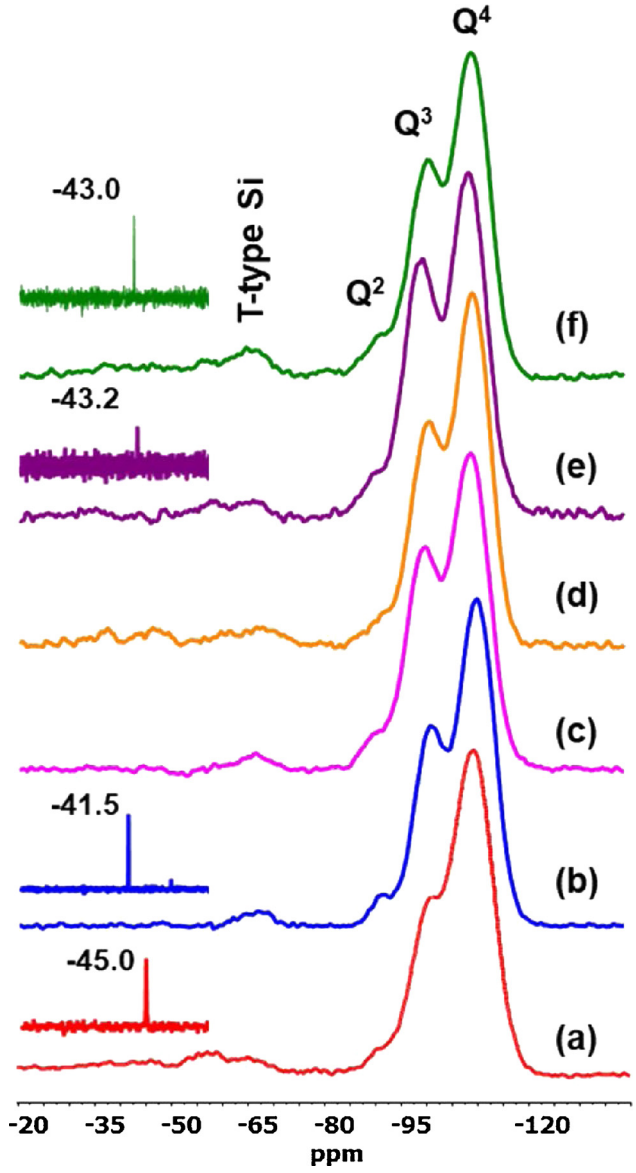

Fig. 3. ^{29}Si BD/MAS NMR spectra of the hybrid base catalyst and the silyl-derivatives counterparts: (a) catalyst **1** and silyl-derivative **I**, (b) catalyst **2** and silyl-derivative **II**, (c) catalyst **3**, (d) catalyst **4**, (e) catalyst **5** and silyl-derivative **V** and (f) catalyst **6** and silyl-derivative **VI**.

Table 2
Functionalized silicon atoms in the mesoporous hybrid materials.

Catalysts	Si_{func}/Si_{tot} (NMR)
Cat. **1**	0.047
Cat. **2**	0.023
Cat. **3**	0.019
Cat. **4**	0.023
Cat. **5**	0.020
Cat. **6**	0.042

3.4.1. Knoevenagel condensation

This reaction can be catalyzed by strong and weak bases, depending on the level of activation of the reactant containing methylenic activated groups which makes it an adequate reaction for comparing catalysts with different basicity. The kinetics of the Knoevenagel reaction is generally considered to be a first order reaction with respect to each reactant and the catalysts. [49–52] Thus, we compared the catalytic performance of hybrid base catalysts **1**-**6** in the Knoevenagel condensation between benzaldehyde and substrates with different pK_a values (with distinct activated methylenic groups), such as ethyl cyanoacetate (pK_a ≈ 9), ethyl acetoacetate (pK_a ≈ 11) and diethyl malonate (pK_a ≈ 13) (Scheme 2). Additionally, a catalytic test of one of the ionic catalysts prior the exchange of I^- for OH- (catalyst **6**, entry **6-I**) was carried out. Lastly, in order to investigate the effect of the surface silanols on the activity of the catalysts, the surface of **1** was passivated with hexamethyldisilazane (HMDS) and the resulting catalyst (**1-HMDS**) was tested.

Firstly, the Knoevenagel condensation between benzaldehyde and ethyl cyanoacetate using the hybrid base catalysts with an active site loading of 10 mol% showed a high activity for the neutral base catalysts **1**-**3** and ionic base catalysts **4**-**6**. Quantitative yields of the final product **A** were achieved with 100% selectivity after 30 min (Table 4, entry 1–6, and Fig. 6).

The same reaction was carried out using catalyst **1-HMDS.** The values show that the catalytic activity decreases giving only a 21% yield after 30 min and longer reaction times of 24 h are required to obtain quantitative yields, emphasizing the vital role the weakly acidic silanols play in reaction (Table 3, entry 7; Fig. 6). [29,30] Moreover, when the reaction was carried out only with MCM-41 a 20% yield was obtained after 24 h, showing that the weakly acidic silanols were able to catalyse the Knoevenagel condensation without the cooperation of the base active site (Table 3, entry 8). Catalyst **6-I** was also tested in the Knoevenagel condensation of ethylcyanoacetate with benzaldehyde. The results show that catalyst **6-I** was not able to catalyse the reaction effectively and after 2 h only a 19% yield is achieved (same activity of the pure silica MCM-41), demonstrating the importance of the hydroxide group to carry out the reaction (Table 3, entry 9, Fig. 6). A blank experiment without any hybrid base catalyst was also performed (Table 3, entry 10), and the data show that the reaction does not occur in the absence of the catalysts.

The Knoevenagel condensation between benzaldehyde and the other two active methylenic substrates with higher pK_a, ethyl acetoacetate and diethyl malonate, to obtain products **B** and **C**, respectively, using the hybrid base catalysts with a catalyst loading of 10 mol % showed a moderate activity of the neutral base catalysts **1**–**3** (Table 3, entry 1–3, Figs. S3, S4). The data showed that in both reactions the best catalysts was **1** and the substrate ethyl acetoacetate (pK_a ≈ 11) was activated more easily than the substrate diethyl malonate (pK_a ≈ 13) giving a 65% yield of the final product **B** and a 45% yield of final product **C** after 24 h, respectively (Table 3, entry 1, Figs. S3, S4). On the contrary, when using the ionic base catalysts **4**-**6** the results show that the reaction does not occur at all (Table 3, entry 4–6). This observation is consistent with an imine or enamine mechanism of the Knoevenagel condensation using a primary or secondary amine base catalyst, respectively. [53]

The proposed reaction imine mechanism promoted by surface silanol groups is given in Scheme 3, using as example catalyst **1** and ethyl cyanoacetate as starting substrate. The catalytic cycle began with the formation of a hydrogen bond between the free silanol group and the oxygen of the carbonyl group of benzaldehyde. Next, the free electron pair of the amine attacked the activated carbonyl group of benzaldehyde, and a carbinolamine was formed through a proton-transfer. This carbinolamine dehydrated, yielding an imine intermediate. The activated methylene get deprotonated by the base to give a stabilized enolate, which then attacked the imine group and generated a new carbon-carbon bond. A rearrangement then ensued that releases the amine base, regenerating the catalyst, and yielding the final olefin product. When the silanol groups were end-capped with trimethylsilyl groups, the initial activation by hydrogen-bonding was absent which resulted in a lower catalytic activity (Table 3, entry 7; Fig. 6). This explained why, when using the hydroxide base catalysts **4–6,** which did not have a primary or a secondary amine group that can be converted into an imine or enamine via aldehyde activation, these were not able

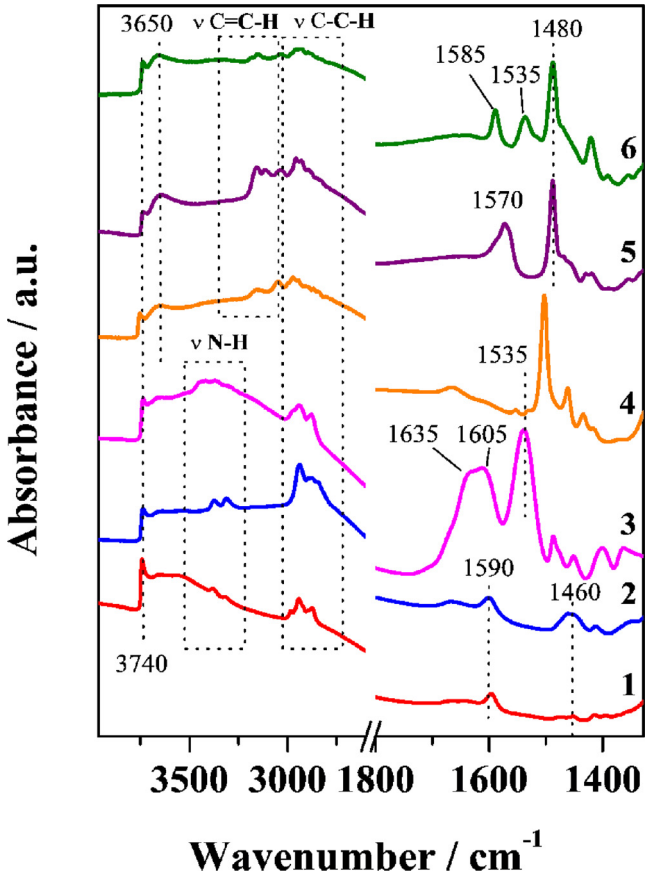

Fig. 4. FTIR spectra of catalysts **1-6** after outgassing at 120 °C.

Table 3
Textural properties of the hybrid base catalysts **1–6.**

Catalysts	SSA_{BET} ($m^2\,g^{-1}$)	Pore volume ($cm^3\,g^{-1}$)
Cat. **1**	973	0.47
Cat. **2**	1159	0.55
Cat. **3**	1005	0.43
Cat. **4**	998	0.45
Cat. **5**	1023	0.46
Cat. **6**	1038	0.44
MCM-41	1064	0.81

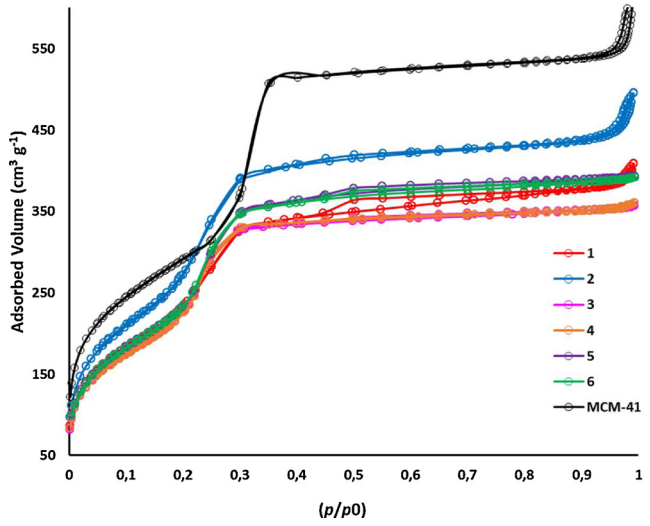

Fig. 5. N_2 adsorption isotherms of the hybrid base catalysts **1-6**.

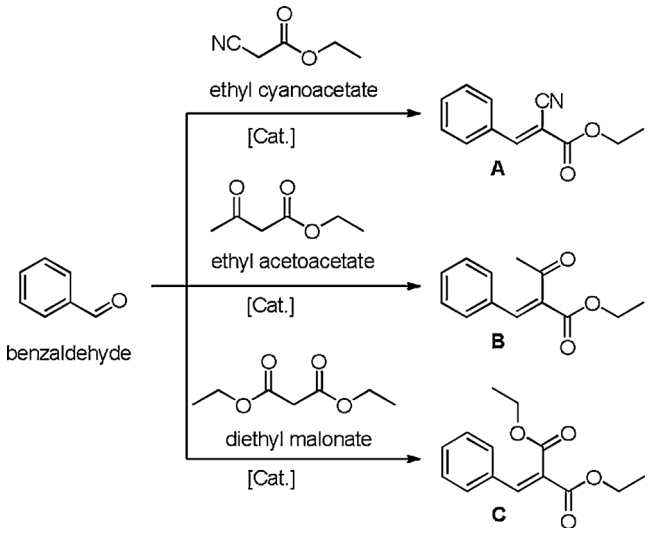

Scheme 2. Scheme of the Knoevenagel reaction of benzaldehyde and ethyl cyanoacetate, ethyl acetoacetate and diethyl malonate.

Table 4
Knoevenagel condensation of benzaldehyde and ethyl cyanoacetate, ethyl acetoacetate and diethyl malonate.

Entry	Catalysts	Yield (%) **A**[a]	Yield (%) **B**[d]	Yield (%) **C**[d]
1	Cat. **1**	93	65	45
2	Cat. **2**	90	63	22
3	Cat. **3**	95	46	18
4	Cat. **4**	91	0	0
5	Cat. **5**	89	0	0
6	Cat. **6**	91	0	0
7	Cat. **1-HMDS**	21	–	–
8	MCM-41[b]	20	–	–
9	Cat. **6-I**[c]	19	–	–
10	None	1	–	–

[a] Reaction conditions: benzaldehyde (1 mmol), ethyl cyanoacetate (1 mmol), ethyl acetoacetate (1 mmol), diethyl malonate (1 mmol) and CH_3CN (4 ml) at 80 °C for 0.5 h with 10 mol % of base sites.
[b] 200 mg of MCM-41, 24 h.
[c] 2 h.
[d] 24 h.

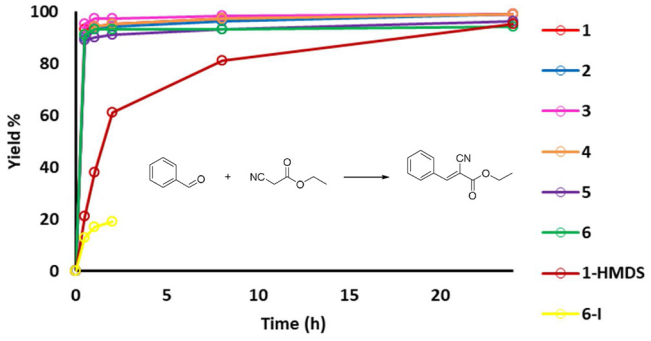

Fig. 6. Catalytic activity of the hybrid base catalysts in the Knoevenagel condensation of benzaldehyde with ethyl cyanoacetate (10 mol % catalyst loading).

to catalyse the reaction between aldehyde and the less active methylenic substrates.

Due to the high activity of the hybrid base catalysts in the Knoevenagel condensation between benzaldehyde and ethyl cyanoacetate to obtain product **A** (Scheme 2), the catalyst loading of the catalyst **1-6** was decreased from 10 mol % to 2 mol % to obtain information about the kinetics of the reaction. Quantitative yields of final

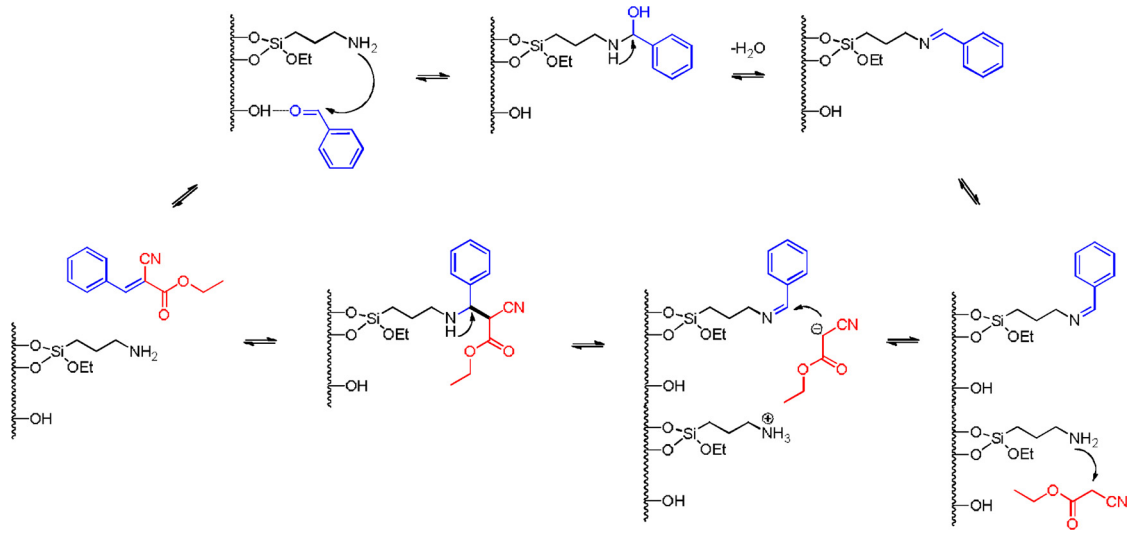

Scheme 3. Proposed enamine catalytic reaction cycle of the Knoevenagel reaction of benzaldehyde and ethyl cyanoacetate, catalyzed by catalyst **1–3**, as an example only catalyst **1** is represented.

Table 5
Knoevenagel condensation of benzaldehyde and ethyl cyanoacetate.

Entry	Catalysts	Time (h)	Yield **A**[a] (%)	TON[b]	TOF[c] (h^{-1})	r_0 ($mol{\cdot}L^{-1}{\cdot}h^{-1}$)	k (h^{-1})
1	Cat. **1**	4	95	48	96	0.49	1.97
2	Cat. **2**	4	93	47	60	0.31	1.24
3	Cat. **3**	4	91	46	56	0.29	1.15
4	Cat. **4**	24	97	49	30	0.16	0.62
5	Cat. **5**	24	95	48	36	0.19	0.74
6	Cat. **6**	24	93	47	46	0.24	0.97

[a] Reaction conditions: benzaldehyde (1 mmol), ethyl cyanoacetate (1 mmol) and CH_3CN (4 ml) at 80 °C with 2 mol % of base sites.
[b] TON calculated at final conversion.
[c] TOF calculated at 15 min.

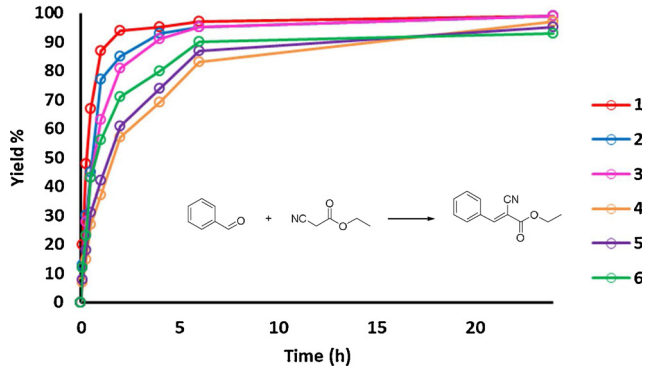

Fig. 7. Catalytic activity of the hybrid base catalysts in the Knoevenagel condensation of benzaldehyde with ethyl cyanoacetate (2 mol % catalyst loading).

product **A** are achieved at around 4 h in the case of neutral base catalyst **1-3**, whereas ionic base catalysts **4–6** needed longer reaction times to accomplish full yield (Table 5, entry 1–3 and 4–6, Fig. 7). As expected, these results followed the catalytic trends shown using 10% mol of catalyst loading (Table 4, Fig. 7). Turnover frequencies calculated after 15 min reaction showed that hybrid base catalyst **1** presented the highest TOF, with a value comparable to those of mesoporous hybrid materials, containing proton sponges (derived of 1,8-bis(dimethylamino)naphthalene (DMAN) compounds). [54] Similarly, initial rates and kinetic constants reported in Table 5 demonstrated that catalytic performance of hybrid base catalysts, specifically catalyst **1**, was comparable with that exhibited by known mesoporous hybrid catalysts, containing base proton sponges (DMAN compounds) into the framework. [54] This comparison confirmed the validity of hybrid base catalysts (catalyst 1) to be used as active base catalysts for C—C bond formation reactions as Knoevenagel condensation.

Catalyst deactivation and reusability were studied in the Knoevenagel condensation between benzaldehyde and ethyl cyanoacetate, using the three most active catalyst **1-3** with 10 mol % of catalyst loading during four successive uses and after 4 h of reaction (Fig. 8). After each experiment, the catalysts were filtered with CH_3CN, washed with acetone, dried at 100 °C, and reused. The yields were similar for the first three catalytic runs, confirming that the hybrid catalysts were recyclable and only a slight loss in activity was observable after four consecutive catalytic uses. XRD diffraction and elemental analysis of the three used hybrid base catalysts **1-3** were carried out to access the stability and integrity of the inorganic framework after four catalytic cycles. The XRD patterns (Fig. S5) show that the first (100) diffraction band characteristic of MCM-41 structure was still present after four consecutive catalytic performances, confirming that the mesoporous MCM-41 morphology was preserved. Moreover, the elemental analysis performed on the three used catalyst **1-3**, revealed that no leaching occurred from 1 to 3 runs whereas after the fourth run an evident loss in the N content was observed, in line with the decrease

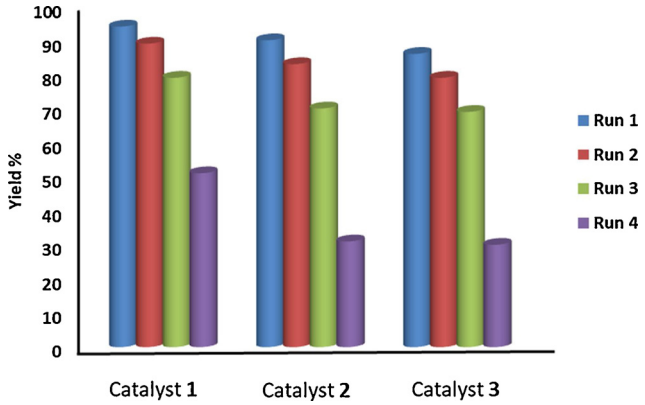

Fig. 8. Recycling tests of Knoevenagel condensation between benzaldehyde and ethyl cyanoacetate (2 mol % catalyst loading). The yield (%) is reported after 4 h of reaction.

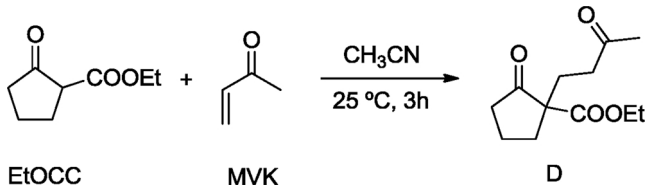

Scheme 4. Scheme of the Michael addition of ethyl 2-oxocyclopentane 2-carboxylate and methyl vinyl ketone.

observed in the yield (Table S1). Additionally, to verify the heterogeneous character of the hybrid base catalysts, a leaching test was performed in the Knoevenagel condensation between benzaldehyde and ethyl cyanoacetate using the three most active catalyst, i.e. **1**-**3,** with 10 mol % of catalyst loading. Thus, when reaction time was 5 min, solid catalysts were filtered from the reaction mixture and the reaction was continued in absence of solid catalyst. After 2 h, a negligible 1% yield increase of the final product was observed (Table S2), proving that no leaching occurs at the condition at which the reaction is carried out.

3.4.2. Michael addition

For the reaction of Michael addition, ethyl 2-oxocyclopentane 2-carboxylate (EtOCC) and methyl vinyl ketone (MVK) were chosen as the donor and the acceptor substrate, respectively (Scheme 4). In all the cases, products coming from side reactions such as rearrangements, dimerizations or other condensations were not observed, and high selectivity to the 1,4-adduct can be achieved. This excellent selectivity must be attributed to the well-defined strong basicity of the ionic base catalysts catalyst **4**-**6**, due to the hydroxide group.

Firstly, the reaction between ethyl 2-oxocyclopentane 2-carboxylate (EtOCC) and methyl vinyl ketone (MVK) was carried using all the hybrid base catalysts **1**-**6** with 5 mol % of catalyst loading at room temperature for 3 h (Scheme 5). For neutral base catalysts **1**-**3** low yields of the final product **D** were achieved (Table 6, entry 1–3). Surprisingly, when using the ionic catalysts **4**-**6** the yields increased up to moderate values in the range of 56–69% yield (Table 6, entry 4–6), evidencing that the hydroxide basicity was crucial to achieve high performances in Michael additions. These three azolium base catalysts presented the positive charge delocalized on the ring conferring more base character

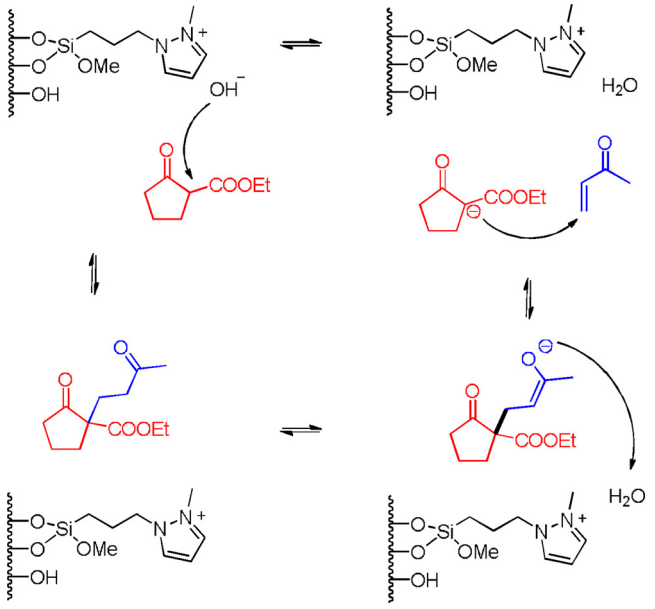

Scheme 5. Proposed enolate catalytic reaction cycle of Michael addition between ethyl 2-oxocyclopentane 2-carboxylate (EtOCC) and methyl vinyl ketone (MVK), catalyzed by catalyst **4–6**, as an example only catalyst **4** is represented.

Table 6
Michael addition of ethyl 2-oxocyclopentane 2-carboxylate and methyl vinyl ketone.

Entry	Catalysts	Yield (%)[a] Time (1 h)	(4 h)	TON[b]
1	**1**	12	19	4
2	**2**	8	9	2
3	**3**	5	8	2
4	**5**	32	56	11
5	**6**	37	63	13
6	**7**	48	69	14
7	**1-HMDS**	7	14	3

[a] Reaction conditions: ethyl 2-oxocyclopentane 2-carboxylate (1 mmol), methyl vinyl ketone (1 mmol) and CH_3CN (0.5 ml) at 25 °C with 5 mol % of base sites.
[b] TON calculated at final conversion.

to the hydroxide groups of the catalysts in the order **4** < **5** < **6**. Pyrazolium base catalyst **4** delocalized the positive charge less effectively than imidazolium base catalyst **5** and **6**, besides dimethyl imidazolium base catalyst **6** presented a electrodonating methyl group that may stabilize the positive charge, conferring more base character to the catalyst than the imidazolium base catalyst **5**. Moreover, these last results compared well with those obtained for solid base catalysts having a hydroxide group. [55] However, the Brönsted basicity of these groups was somewhat lower than when they are unsupported [55].

Finally, the same reaction was carried out using catalyst **1-HMDS** not having free silanols to prevent acid-base cooperative catalysis. The values show that the catalytic activity decreases achieving only a 14% yield after 4 h, confirming that the weakly acidic silanols also play an important role in Michael additions (Table 6, entry 7).

For Michael additions an enolate mechanism was proposed where the ionic base catalysts are the best candidates to catalyse this reaction due to the stronger basicity conferred by the hydroxide groups. [56] The proposed reaction enolate mechanism is shown in Scheme 5, using as example catalyst **3**. The catalytic cycle began with the deprotonation of the methylenic active substrate (EtOCC) by the hydroxide group that lead to the enolate ion. Next, this nucleophile reacted with the electrophilic alkene (MVK) to form a new carbon-carbon bond. Proton abstraction from the protonated base by the enolate achieved the final Michael addition product.

4. Conclusions

Hybrid mesoporous base materials, synthesized by means of post-grafting procedures and containing neutral (amine, diamine, pyrrolidine) or ionic (pyrazolium, imidazoliun) base sites, have been successfully synthesised and evaluated in different catalytic transformations. The characterisation of the hybrids has revealed that the organic bases were preserved inside the mesoporous silica network, providing strong base properties to the hybrid materials. These hybrid catalysts were tested in the Knoevenagel condensation and Michael addition, respectively. In particular, for Knoevenagel condensation, the neutral base catalysts showed higher catalytic activity with respect to the other ionic hybrids. This superior activity could be justified by the imine and enamine mechanism of the reaction that was favoured with the presence of primary and secondary amine, respectively. Additionally, the presence of silanols groups in the framework of the support would perform a cooperative electrophilic activation. On the other hand, for Michael addition, the ionic base catalysts were more efficient than the neutral base catalysts, suggesting that an enolate mechanism was taking place and it was favoured when hydroxide groups were present as base sites. The achieved results show that the synthesis method to generate active hybrid materials opens the possibility of combining these base sites with other acid and/or redox structural functions to generate multisite catalysts for carrying out cascade type or one-pot multistep

catalytic processes.

Acknowledgments

The authors are grateful for financial support from the Spanish Government by MAT2017-82288-C2-1-P and Severo Ochoa Excellence ProgramSEV-2016-0683. The authors thank the MULTY2HYCAT (EU-Horizon 2020 funded project under grant agreement no. 720783). A. E. acknowledges “La Caixa” foundation for PhD scholarship.

Appendix A. Supplementary data

Supplementary material related to this article can be found, in the online version, at doi:https://doi.org/10.1016/j.cattod.2019.09.041.

References

[1] U. Diaz, D. Brunel, A. Corma, Chem. Soc. Rev. 42 (2013) 4083–4097.
[2] G. Ferey, Chem. Soc. Rev. 37 (2008) 191–214.
[3] D.A. Loy, K.J. Shea, Chem. Rev. 95 (1995) 1431–1442.
[4] F. Hoffmann, M. Cornelius, J. Morell, M. Fröba, Angew. Chem. Int. Ed. 45 (2006) 3216–3251.
[5] A.P. Wight, M.E. Davis, Chem. Rev. 102 (2002) 3589–3614.
[6] K. Vallé, P. Belleville, F. Pereira, C. Sanchez, Nat. Mater. 5 (2006) 107–111.
[7] B. Boury, R.J.P. Corriu, Chem. Commun. (2002) 795–802.
[8] A. Mehdi, C. Reye, R.J.P. Corriu, Chem. Soc. Rev. 40 (2011) 563–574.
[9] C. Sánchez, B. Julián, P. Belleville, M. Popall, J. Mater. Chem. 15 (2005) 3559–3592.
[10] C. Sánchez, F. Ribot, New J. Chem. 18 (1994) 1007–1047.
[11] C. Sánchez, L. Rozes, F. Ribot, C. Laberty-Robert, D. Grosso, C. Sassoye, C. Boissiere, L. Nicole, C. R. Chim. 13 (2010) 3–39.
[12] J.W. Park, Y.J. Park, C.H. Jun, Chem. Commun. 47 (2011) 4860–4871.
[13] J. Lauwaert, E. De Canck, D. Esquivel, J.W. Thybaut, P. Van Der Voort, G.B. Marin, ChemCatChem 6 (2013) 255–264.
[14] H. Yuan, W.J. Yoo, H. Miyamura, S.S. Kobayashi, J. Am. Chem. Soc. 134 (2012) 13970–13973.
[15] M.W. McKittrick, C.W. Jones, Chem. Mater. 15 (2003) 1132–1139.
[16] M.W. McKittrick, C.W. Jones, J. Am. Chem. Soc. 126 (2004) 3052–3053.
[17] R.K. Zeidan, S.J. Hwang, M. Davis, Angew. Chem. Int. Ed. 45 (2006) 6332–6335.
[18] N.A. Brunelli, K. Venkatasubbaiah, C.W. Jones, Chem. Mater. 24 (2012) 2433–2442.
[19] J. Lauwaert, E.G. Moschetta, P. Van Der Voort, J.W. Thybaut, C.W. Jones, G.B. Marin, J. Catal. 325 (2015) 19–25.
[20] J.D. Bass, A. Solovyov, A.J. Pascall, A. Katz, J. Am. Chem. Soc. 128 (2006) 3737–3747.
[21] J. Lauwaert, E. De Canck, D. Esquivel, J.W. Thybaut, P. Van Der Voort, G.B. Marin, ChemCatChem 6 (2014) 255–264.
[22] K.K. Sharma, R.P. Buckley, T. Asefa, Langmuir 24 (2008) 14306–14320.
[23] V.E. Collier, N.C. Ellebracht, G.I. Lindy, E.G. Moschetta, C.W. Jones, ACS Catal. 6 (2016) 460–468.
[24] N.A. Brunelli, K. Venkatasubbaiah, C.W. Jones, Chem. Mater. 24 (2012) 2433–2442.
[25] T.Y. Ma, H. Li, Q.F. Deng, L. Liu, T.Z. Ren, Z.Y. Yuan, Chem. Mater. 24 (2012) 2253–2255.
[26] K.C. Kim, E.G. Moschetta, C.W. Jones, S.S. Jang, J. Am. Chem. Soc. 138 (2016) 7664–7672.
[27] N.A. Brunelli, C.W. Jones, J. Catal. 308 (2013) 60–72.
[28] N.A. Brunelli, K. Venkatasubbaiah, C.W. Jones, J. Am. Chem. Soc. 134 (2012) 13950–13953.
[29] A. Vylder, J. Lauwaert, D. Esquivel, D. Poelman, J. De Clercq, P. Van Der Voort, Joris W. Thybaut, J. Catal. 361 (2018) 51–61.
[30] J.D. Bass, A. Solovyov, A.J. Pascall, A. Katz, J. Am. Chem. Soc. 128 (2006) 3737–3747.
[31] N.A. Brunelli, C.W. Jones, Catalysis 308 (2013) 60–72.
[32] S.J. Gregg, K.S.W. Sing, Adsorption, Surface Area and Porosity, Academic Press, London, 1982.
[33] K.S.W. Sing, D.H. Everett, R.A.W. Haul, L. Moscou, R.A. Pierotti, J. Rouquerol, T. Siemieniewska, Pure Appl. Chem. 57 (1985) 603–619.
[34] E.P. Barrett, L.G. Joyner, P.P. Halenda, J. Am. Chem. Soc. 73 (1951) 373–380.
[35] R. Mokaya, W. Jones, J. Mater. Chem. 8 (1998) 2819–2826.
[36] P.T. Tanev, T.J. Pinnavaia, Science 267 (1995) 865–867.
[37] K. Kawahara, Y. Hagiwara, A. Shimojima, K. Kuroda, J. Mater. Chem. 18 (2008) 3193–3195.
[38] G. Socrates, Infrared Charecteristics Group Frequencies, John Wiley and Sons, 1980.
[39] B. Haddad, D. Mokhtar, M. Goussem, E. Belarbi, D. Villemin, S. Bresson, M. Rahmouni, N.R. Dhumal, H.J. Kim, J. Kiefer, J. Mol. Struct. 1134 (2017) 582–590.
[40] I. Rodríguez, S. Iborra, F. Rey, J.L. Jordá, A. Corma, Chem. Commun. (1999) 593–594.
[41] M.J. Climent, A. Corma, S. Iborra, K. Epping, A. Velty, J. Catal. 225 (2004) 316–326.
[42] F.S. Prout, V.D. Beaucaire, G.R. Dyrkacz, W.M. Koppes, R.E. Kuznicki, T.A. Marlewski, J.J. Pienkowski, J.M. Puda, J. Org. Chem. 38 (1973) 1512–1517.
[43] G. Jones, Org. React. 15 (2011) 204–599.
[44] J. Guyot, A. Kergomard, Tetrahedron 39 (1983) 1167–1179.
[45] W. Lubisch, E. Beckenbach, S. Bopp, H.-P. Hofmann, A. Kartal, C. Kästel, T. Lindner, M. Metz-Garrecht, J. Reeb, F. Regner, M. Vierling, A. Möller, J. Med. Chem. 46 (2003) 2404–2412.
[46] N. Vlok, S.F. Malan, N. Castagnoli, J.J. Bergh, J.P. Petzer, Bioorg. ed. Chem. 14 (2006) 3512–3521.
[47] C. Selvam, S.M. Jachak, R. Thilagavathi, A.K. Chakraborti, Bioorg. Med. Chem. Lett. 15 (2005) 1793–1797.
[48] K. Nakayama, Y. Ishida, M. Ohtsuka, H. Kawato, K.-i. Yoshida, Y. Yokomizo, S. Hosono, T. Ohta, K. Hoshino, H. Ishida, K. Yoshida, T.E. Renau, R. Léger, J.Z. Zhang, V.J. Lee, W. Watkins, J. Bioorg. Med. Chem. Lett. 13 (2003) 4201–4204.
[49] S. Inagaki, S. Guan, T. Ohsuna, O. Terasaki, Nature 416 (2002) 304–307.
[50] J. Jung, C. Jo, K. Cho, R. Ryoo, Mater. Chem. 22 (2012) 4637–4640.
[51] G. Bellussi, E. Montanari, E. Di Paola, R. Millini, A. Carati, C. Rizzo, W. O'Neil Parker, M. Gemmi, E. Mugnaioli, U. Kolb, S. Zanardi, Angew. Chem. Int. Ed. 51 (2012) 666–669.
[52] A. Gaona, J.M. Moreno, A. Velty, U. Diaz, A. Corma, J. Mater. Chem. A 2 (2014) 19360–19375.
[53] E. Knoevenagel, Ber. Dtsch. Chem. Ges. 31 (1898) 2596–2619.
[54] A. Corma, S. Iborra, I. Rodríguez, F. Sánchez, J. Catal. 211 (2002) 208–215.
[55] I. Rodríguez, S. Iborra, F. Rey, A. Corma, Appl. Catal. A 194 – 195 (2000) 241–252.
[56] R.D. Little, M.R. Masjedizadeh, O. Wallquist, J.I. McLoughlin, Org. React. 47 (1995) 315–552.